
Row-clustering of a Point Process-valued Matrix

Lihao Yin¹, Ganggang Xu², Huiyan Sang¹, Yongtao Guan²

¹Department of Statistics, Texas A&M University

²Department of Management Science, University of Miami

¹{Lihao,Huiyan}@stat.tamu.edu,²{gangxu,yguan}@bus.miami.edu

Abstract

Structured point process data harvested from various platforms poses new challenges to the machine learning community. To cluster repeatedly observed marked point processes, we propose a novel mixture model of multi-level marked point processes for identifying potential heterogeneity in the observed data. Specifically, we study a matrix whose entries are marked log-Gaussian Cox processes and cluster rows of such a matrix. An efficient semi-parametric Expectation-Solution (ES) algorithm combined with functional principal component analysis (FPCA) of point processes is proposed for model estimation. The effectiveness of the proposed framework is demonstrated through simulation studies and real data analyses.

1 Introduction

Large-scale, high-resolution, and irregularly scattered event time data has attracted enormous research interest recently in many applications, including medical visiting records [14], financial transaction ledgers [32] and server logs [12]. Given a collection of event time sequences, one research thread is to identify groups displaying similar patterns. In practice, the significance of this task emerges in multifarious scenarios. For example, matching users with similar activity patterns on social media platforms is beneficial to ads recommendations; clustering patients by their visiting records may help predict the course of the disease progression.

Our study is motivated by a dataset we collected from Twitter, which consists of posting times of 500 university official accounts from April 15, to May 14th, 2021. Figure 1 displays posting time stamps of seven selected accounts in five consecutive days. While the daily posting patterns vary across different accounts, the posting date seems to also play an important role. Specifically, all accounts cascade a barrage of postings on April 16th while few postings appear on April 18th. Lastly, each posting is associated with a specific type of activity, namely, tweet, retweet, or reply. Our main interest is to cluster these multi-category, dynamic posting patterns into subgroups.

To characterize the highly complex posting patterns, we propose a mixture model of Multi-level Marked Point Processes (MM-MPP). We assume that the event sequences from each cluster are realizations of a multi-level log-Gaussian Cox process (LGCP) [19], which has been demonstrated useful for modeling repeatedly observed event sequences [32]. We here extend their work to the case of mixture models and propose a semiparametric Expectation-Solution algorithm to learn the underlying cluster structure. The proposed learning algorithm avoids iterative numerical optimizations within each ES step and hence is computationally efficient. In particular, the expectation step is carried out using MCMC samples based on the FPCA of the latent Gaussian processes, which imposes minimal parametric assumptions on the proposed model. Finally, we design an algorithm that can take advantage of array programming and GPU acceleration to further speed up computation.

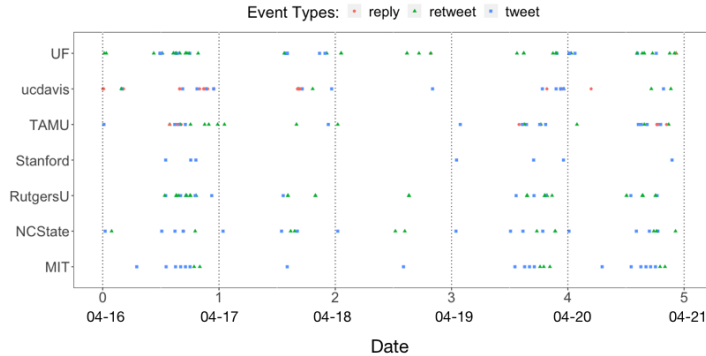


Figure 1: The activities of selected accounts on Twitter.

2 Related Work

Modelling of Event Sequences Point processes have been widely used to model temporal events [6], although rarely does existing work focus on repeatedly observed event sequences. One prominent example is the Hawkes process [9, 36, 37], which accounts for temporal dependence among events by a self-triggering mechanism. However, the existing Hawkes process may fail to describe our cases for two reasons. First, many human activities naturally have discontinuity by day. So it is unclear how to define the triggering mechanism across days with Hawkes processes. Second, the multivariate Hawkes process characterizes an overall rate of events for different days. The clustering methods based on the Hawkes process [17, 16, 34] are more likely to distinguish individuals by overall event frequency, other than their intra-day behavior patterns.

In our motivating example, there exist multiple variations for the event sequences, both from individual and day levels. One way to account for variations from multiple sources is to exploit Cox process models, whose intensities are modeled by latent random functions. One popular class of Cox processes is the log-Gaussian Cox process (LGCP) [19], whose latent intensity functions are assumed to be transformed Gaussian processes. Recently, [32] proposed a multi-level LGCP model to account for different sources of variations for repeatedly observed event data. However, clustering of repeatedly observed marked event time data was not considered in their work.

Clustering of Event Sequences. Extensive research has been done on this topic. To our knowledge, clustering models for point processes can be summarized into two major categories: distance-based clustering [3, 4, 22] and distribution-based clustering [34, 17]. The former measures the closeness between event sequences based on some extracted features and then uses classical distance-based clustering algorithms such as k -means [4, 23] or EM algorithms [31]. The second approach, also referred to as model-based clustering, assumes that event sequences are derived from a parametric mixture model of point processes. One notable thread is the mixture model of the Hawkes point processes. For example, [34] proposed a Dirichlet mixture of Hawkes processes (DMHP) under the Expectation-Maximization (EM) framework to identify clusters. However, existing EM algorithms for event sequence clustering have a common issue that they typically require iterative numerical optimizations within each M-step, which would drastically overburden the computation. This computational issue will be accentuated when event data are repeatedly observed and have marks.

3 Model-based Row-clustering for a Matrix of Marked Point Processes

Notation. Suppose that we observe daily event sequences from n accounts during m days. For account i on day j , let $N_{i,j}$ denote the total number of events, $t_{i,j,l} \in (0, T)$ denote the l -th event time stamp, and $r_{i,j,l} \in \{1, \dots, R\}$ denote the corresponding event types (marks). The activities of account i on day j can be summarized by a set $S_{i,j} = \{(t_{i,j,l}, r_{i,j,l})\}_{l=1}^{N_{i,j}}$, recording the time stamps and types for all $N_{i,j}$ events. This general notation can also describe other marked event sequences which are repeatedly observed on m non-overlapping time slots. We represent the collection of all marked daily event sequences as an $n \times m$ matrix \mathcal{S} , whose (i, j) th entry is a marked event sequence

$S_{i,j}$. We aim to cluster the rows of \mathcal{S} to identify potential heterogeneity in account activity patterns, while taking into account the dependence across rows and columns to characterize the complex event patterns and interactions among accounts, days, and event types.

3.1 A Mixture of Multi-level Marked LGCP Model

Given a matrix of daily event sequences \mathcal{S} , we can separate each matrix entry $S_{i,j}$ according to their marks (event types). Let $S_{i,j}^r = \{t_{i,j,l} | r_{i,j,l} = r\}$ be the collection of time stamps of event type $r \in \{1, \dots, R\}$. We model each $S_{i,j}^r$ by an inhomogeneous Poisson point process conditional on a latent intensity function $\lambda_{i,j}^r(t | \Lambda_{i,j}^r) = \exp\{\Lambda_{i,j}^r(t)\}$, where $\Lambda_{i,j}^r(t) : [0, T] \mapsto \mathbb{R}$ is the random log intensity function on $[0, T]$. Following [32], we assume a multi-level model for $\Lambda_{i,j}^r(t)$:

$$\Lambda_{i,j}^r(t) = X_i^r(t) + Y_j^r(t) + Z_{i,j}^r(t), \quad t \in [0, T], \quad (1)$$

for $i = 1, \dots, n$, $j = 1, \dots, m$ and $r = 1, \dots, R$. In model (1), $X_i^r(t)$, $Y_j^r(t)$ and $Z_{i,j}^r(t)$ are random functions on $[0, T]$, characterizing the variations of account-level, day-level and the residual deviations, respectively. In addition, we also take into account the dependence across event types when modelling $X_i^r(t)$, $Y_j^r(t)$ and $Z_{i,j}^r(t)$, while assuming independence across accounts, that is, for any (r, r') , $X_i^r(t)$ and $X_{i'}^{r'}(t)$ are independent when $i \neq i'$, $Y_j^r(t)$ and $Y_{j'}^{r'}(t)$ are independent when $j \neq j'$, and $Z_{i,j}^r(t)$ and $Z_{i',j'}^{r'}(t)$ are independent if $(i, j) \neq (i', j')$.

We assume that $\mathbf{X}_i(t) = \{X_i^r(t)\}_{r=1}^R$ is a mixture of multivariate Gaussian processes with C components in order to detect heterogeneous clusters. We introduce a binary vector $\boldsymbol{\omega}_i = \{\omega_{1,i}, \dots, \omega_{C,i}\}'$ to encode the cluster membership for account i , where $\omega_{c,i} = 1$ if account i belongs to the c -th cluster and 0 otherwise. In analogy to other model-based clustering approaches, the unobserved cluster membership $\boldsymbol{\omega}_i$ are treated as missing data and assumed to follow a categorical distribution with parameter $\boldsymbol{\pi} = \{\pi_1, \dots, \pi_C\}$, where π_c indicates the probability that an account belongs to the c -th cluster. Conditional on $\boldsymbol{\pi}$, we assume that $X_i^r(t)$'s in different clusters have heterogeneous behavioral patterns, characterized by their corresponding cluster-specific multivariate Gaussian processes with mean functions $\mu_{x,c}^r(t) = \mathbb{E}[X_i^r(t) | \omega_{c,i} = 1]$ and cross covariance functions $\Gamma_{x,c}^{r,r'}(s, t) = \text{Cov}[X_i^r(s), X_i^{r'}(t) | \omega_{c,i} = 1]$, for $s, t \in [0, T]$, and $r, r' = 1, \dots, R$. Here, $\mu_{x,c}^r(t)$ characterizes the cluster-specific first-order intensity function, and $\Gamma_{x,c}^{r,r'}(s, t)$ describes the temporal dependence patterns within and across event types in the same cluster c , $c = 1, \dots, C$.

Similarly, we assume that $\mathbf{Y}_j(t) = \{Y_j^r(t)\}_{r=1}^R$ and $\mathbf{Z}_{i,j}(t) = \{Z_{i,j}^r(t)\}_{r=1}^R$ are both mean-zero multivariate Gaussian processes to account for dependence of day-level and residual random effects within and across event types, respectively. The covariance functions take the forms: $\Gamma_y^{r,r'}(t) = \text{Cov}[Y_j^r(t), Y_j^{r'}(t)]$, and $\Gamma_z^{r,r'}(t) = \text{Cov}[Z_{i,j}^r(t), Z_{i,j}^{r'}(t)]$. As the heterogeneity patterns are assumed to be mainly explained by the account-level effect \mathbf{X} , both $\Gamma_y^{r,r'}(t)$ and $\Gamma_z^{r,r'}(t)$ are assumed to be homogeneous across all clusters.

A Single-level Special Case. When $m = 1$, our data matrix \mathcal{S} only has one column of event sequences. The multi-level model in (1) reduces to a single-level model:

$$\lambda_{i,1}^r(t | \Lambda_{i,1}^r) = \exp\{\Lambda_{i,1}^r(t)\}, \quad \Lambda_{i,1}^r = X_i^r(t), \quad t \in [0, T] \quad (2)$$

where $\mathbf{X}_i(t) = \{X_i^r(t)\}_{r=1}^R$ has the same model specification as in the multi-level case described earlier. We remark that it is still of importance to consider this special case that has also been studied in the literature [33], as even in this simpler case limited work has been done for the clustering of repeatedly observed marked point processes.

3.2 Likelihood Function

We denote the parameters concerning $\mathbf{X}_i(t)$ in cluster c as $\Theta_{x,c}$ and the parameters concerning $Y_j(t)$ and $Z_{i,j}(t)$ as Θ_y and Θ_z , respectively. Therefore, the parameters in model (1) consist of $\Omega = \{\boldsymbol{\pi}, \Theta_y, \Theta_z, \Theta_{x,c}, c = 1, \dots, C\}$. When $m = 1$, $\Omega = \{\boldsymbol{\pi}, \Theta_{x,c}, c = 1, \dots, C\}$ representing the parameters involved in model (2). The complete data \mathcal{D} consists of the observed data \mathcal{S} and the unobserved latent variables $\{\{\boldsymbol{\omega}_i\}_{i=1}^n, \mathcal{L}\}$, where $\mathcal{L} = \{\{\mathbf{X}_i(t)\}, \{\mathbf{Y}_i(t)\}, \{\mathbf{Z}_{i,j}(t)\}\}$ for model (1)

and $\mathcal{L} = \{\{\mathbf{X}_i(t)\}\}$ for model (2). Let S_i be the i -th row of \mathcal{S} representing activities of the i -th account. In our mixture model, the probability of the observed data \mathcal{S} can be written as

$$p(\mathcal{S}; \Omega) = \mathbb{E}_{\omega} \mathbb{E}_{\mathcal{L}} \left[\prod_{i=1}^n \text{PP}(S_i | \mathcal{L}) \mid \{\omega_i\}_{i=1}^n; \Omega \right], \quad (3)$$

where the expectations are taken with respect to the conditional distribution of latent variables \mathcal{L} and ω_i 's, and $\text{PP}(S_i | \mathcal{L})$ is the conditional probability of a Poisson point process,

$$\text{PP}(S_i | \mathcal{L}) = \prod_{j=1}^m \prod_{r=1}^R \left\{ \prod_{t \in S_{i,j}^r} \lambda_{i,j}^r(t | \Lambda_{i,j}^r) \exp \left[- \int_0^T \lambda_{i,j}^r(s | \Lambda_{i,j}^r) ds \right] \right\}, \quad (4)$$

where, conditional on \mathcal{L} , $\Lambda_{i,j}^r(t)$ has the form as (1) for $m > 1$ and as (2) for $m = 1$.

4 Row-clustering Algorithms

Existing mixture model-based clustering methods typically rely on likelihood-based Expectation-Maximization algorithms [1] by treating unobserved latent variables, $\{\{\omega_i\}_{i=1}^n, \mathcal{L}\}$ in our case, as missing data. However, standard EM algorithms are computationally intractable for the models we consider here. One computation bottleneck is the numerical optimizations involved in M-steps, which require many iterations due to the lack of closed-form solutions when updating parameters. Moreover, the computation burden is severely aggravated by the fact that the expectations in E-step (see (3) for an example) involve an intractable multivariate integration.

In Section 4.1, we describe a novel efficient semi-parametric Expectation-Solution algorithm for the single-level model in (2) to bypass the computation challenges described above. We then show in Section 4.2 that the learning task of multi-level models in (1) can be transformed and solved by utilizing an algorithm similar to that of single-level models.

4.1 Learning of Single-level Models

The ES algorithm [7] is a general iterative approach to solving estimating equations involving missing data or latent variables. The algorithm proceeds by first constructing estimating equations based on a complete-data summary statistic, which may arise from a likelihood, a quasi-likelihood, or other generalized estimating equations. Similar to the EM algorithm, the ES algorithm then iterates between an expectation (E)-step and a solution (S)-step until convergence to obtain parameter estimates. The detailed steps of a general ES algorithm framework are included in Supplementary S.2. The EM framework is a special case of ES when estimating equations are constructed from full likelihoods and using complete data as the summary statistic.

Due to the lack of closed-form for the likelihood function (3), we opt to design our algorithm under the more flexible and general ES framework for parameter estimations of the single-level models in (2), i.e., $m = 1$. The algorithm is summarized in Algorithm 1 and detailed below.

As a preliminary, we give the form of the expectation of the conditional intensity function given cluster memberships as follows:

$$\rho_c^r(t) = \mathbb{E}[\lambda_{i,1}^r(t) \mid \omega_{c,i} = 1] = \exp[\mu_{x,c}^r(t) + \Gamma_{x,c}^r(t, t)/2]. \quad (5)$$

The form of the second-order conditional intensity function is

$$\begin{aligned} \rho_{c,i}^{r,r'} &= \mathbb{E}[\lambda_i^r(s) \lambda_i^{r'}(t) \mid \omega_{c,i} = 1] = \mathbb{E}\{\exp[X_i^r(s) + X_i^{r'}(t) \mid \omega_{c,i} = 1]\} \\ &= \rho_c^r(s) \rho_c^{r'}(t) \exp[\Gamma_{x,c}^{r,r'}(s, t)], \end{aligned} \quad (6)$$

for $i = 1, \dots, n$, $r, r' = 1, \dots, R$, where the last equality is derived following the moment generating function of a Gaussian random variable.

Estimating Equations. We carefully construct estimating equations of unknown parameters with three considerations in mind: (1) the expectation of the estimating equations over the complete data should be zero; (2) the conditional expectation of the estimating equation can be solved efficiently in the S-step; (3) the estimating equations should be fast to calculate.

Let $K(\cdot)$ be a kernel function and $K_h(t) = h^{-1}K(t/h)$ with a bandwidth $h > 0$. We define

$$A_c^{r,r'}(s, t; h) = \sum_{i=1}^n \omega_{c,i} a_i^{r,r'}(s, t; h), \quad \text{where } a_i^{r,r'}(s, t; h) = \sum_{u \in S_i^r} \sum_{v \in S_i^{r'}} \frac{K_h(s-u)K_h(t-v)}{ng(s;h)g(t;h)};$$

$$B_c^r(t; h) = \sum_{i=1}^n \omega_{c,i} b_i^r(t; h), \quad \text{where } b_i^r(t; h) = \sum_{u \in S_i^r} \frac{K_h(t-u)}{ng(t;h)}, \quad (7)$$

for $c = 1, \dots, C$, and $r, r' = 1, \dots, R$, where $g(x; h) = \int K_h(x-t)dt$. Using the Campbell's Theorem [20] and the moment generating function of the normal distribution, it is straightforward to show that $\mathbb{E}[A_c^{r,r'}(s, t; h)|\boldsymbol{\omega}] \approx \pi_c \rho_c^r(s) \rho_c^{r'}(t) \exp[\Gamma_{x,c}^{r,r'}(s, t)]$ and that $\mathbb{E}[B_c^r(t; h)|\boldsymbol{\omega}] \approx \pi_c \rho_c^r(t)$, provided that h is sufficiently small. This motivates us to consider the following estimating equations:

$$\begin{cases} A_c^{r,r'}(s, t; h) - \pi_c \rho_c^r(s) \rho_c^{r'}(t) \exp[\Gamma_{x,c}^{r,r'}(s, t)] = 0 \\ B_c^r(t; h) - \pi_c \rho_c^r(t) = 0 \\ n^{-1} \sum_{i=1}^n \omega_{c,i} - \pi_c = 0. \end{cases} \quad (8)$$

Expectation (E-step). Given an observed data \mathcal{S} and a current parameter estimate Ω^* , we calculate the conditional expectation of the estimation equations in (8). Note that, conditioned on \mathcal{S} , the three estimating equations are all linear with respect to $\{\omega_{c,i}, c = 1, \dots, C, i = 1, \dots, n\}$. Therefore, the conditional expectations of the estimating equations are obtained by replacing $\omega_{c,i}$ with its conditional expectation $\mathbb{E}_\omega[\omega_{c,i}|\mathcal{S}; \Omega^*]$, which has the following form:

$$\mathbb{E}_\omega[\omega_{c,i}|\mathcal{S}; \Omega^*] = \frac{\pi_c^* f(S_i|\omega_{c,i} = 1; \Omega^*)}{\sum_{c=1}^C \pi_c^* f(S_i|\omega_{c,i} = 1; \Omega^*)}, \quad (9)$$

where $f(S_i|\omega_{c,i} = 1; \Omega^*) = \mathbb{E}_\mathcal{L}[\text{PP}(S_i|\mathcal{L})|\omega_{c,i} = 1; \Omega^*]$. Here $\text{PP}(\cdot)$ is the conditional distribution function of S_i given $\omega_{c,i}$ and Ω^* as defined in (4). We propose to approximate $f(S_i|\omega_{c,i} = 1; \Omega^*)$ by its Monte Carlo counterpart,

$$\hat{f}(S_i | \omega_{c,i} = 1; \Omega^*) \approx Q^{-1} \sum \hat{\text{PP}}(S_i | \mathbf{X}_c^{(q)}(t)), \quad (10)$$

where Q is the Monte Carlo sample size, $\mathbf{X}_c^{(q)}(t)$'s are independent samples from the multivariate Gaussian process with parameters $\Theta_{x,c}^*$ (see details below), and $\hat{\text{PP}}(\cdot)$ is a numerical quadrature approximation of $\text{PP}(\cdot)$ following [2]:

$$\hat{\text{PP}}(S_i|\mathbf{X}(t)) = \exp \left\{ \sum_{r=1}^R \sum_{u \in \tilde{S}_{i,1}^r} v_u [y_u X^r(u) - \exp X^r(u)] \right\}, \quad (11)$$

In the above, $\tilde{S}_{i,1}^r$ is the union of $S_{i,1}^r$ and a set of regular grid points, v_u is the quadrature weight corresponding to each u and $y_u = v_u^{-1} \Delta_u$, where Δ_u is an indicator of whether u is an observation ($\Delta_u = 1$) or a grid point ($\Delta_u = 0$).

Solution (S-step). In this step, we update the parameters by finding the solutions to the expected estimating equations from the E-step. For $c = 1, \dots, C$, $r, r' = 1, \dots, R$ and $r \neq r'$, the solutions take the following closed forms:

$$\pi_c^* = n^{-1} \sum_{i=1}^n \mathbb{E}[\omega_{c,i}|\mathcal{S}; \Omega^*], \quad (12)$$

$$\Gamma_{x,c}^{r,r'*}(s, t) = \log \frac{\pi_c^* \mathbb{E}_\omega[A_c^{r,r'}(s, t; h)|\mathcal{S}; \Omega^*]}{\mathbb{E}_\omega[B_c^r(s; h)|\mathcal{S}; \Omega^*] \mathbb{E}_\omega[B_c^{r'}(t; h)|\mathcal{S}; \Omega^*]}, \quad (13)$$

$$\mu_{x,c}^{r'*}(t) = \log \left\{ \pi_c^{*-1} \mathbb{E}_\omega[B_c^r(t; h)|\mathcal{S}; \Omega^*] / \exp[\Gamma_{x,c}^{r'*}(t, t)/2] \right\}. \quad (14)$$

Sampling Strategies. The multi-dimensional functional form of $\mathbf{X}_c^{(g)}$ renders the sampling procedures in (10) intractable. Given $\Theta_{x,c}$, one solution is to find a low-rank representation of \mathbf{X}_i with the functional principal components analysis (FPCA) [24]. Specifically, we approximate the latent Gaussian process \mathbf{X}_i in cluster c nonparametrically using the Karhunen-Lòeve expansion [29] as: $X_i^r(t) = \boldsymbol{\mu}_c + \boldsymbol{\xi}_i^T \boldsymbol{\phi}(t)$, for $r = 1, \dots, R$, where $\boldsymbol{\xi}_i$ is a vector of normal random variables, and $\boldsymbol{\phi}(t)$ is a vector of orthogonal eigenfunctions. Using FPCA, we can obtain the samples of \mathbf{X}_i by sampling $\boldsymbol{\xi}_i$ indirectly. More detailed sampling procedure via FPCA can be seen in Supplementary S.2.

Remarks. The most significant advantage of our method is that it avoids expensive iterations inside each E-step and S-step, unlike other EM algorithms for mixture point process models [34]. The elements $a_i^{r,r'}(s, t; h)$'s and $b_i^r(t; h)$'s in (7) can be pre-calculated before E-S iterations to save computations. Moreover, the S-step is fast to execute thanks to the closed-form solutions. We will analyze the overall computation complexity of the learning algorithm in Section 4.3.

Algorithm 1 Learning of the Single-level model in (2)

Input: $\mathcal{S} = \{S_i\}_{i=1}^n$, the number of clusters C , the bandwidth h ;

Output: Estimates of model parameters, $\hat{\boldsymbol{\pi}}, \hat{\mu}_{x,c}^r(t), \hat{\Gamma}_{x,c}^{r,r'}(s, t)$, for $c = 1, \dots, C, r, r' = 1, \dots, R$;

Calculate the components $a_i^{r,r'}(s, t; h)$'s and $b_i^r(t; h)$'s given in (7);

Initialize $\Omega^* = \{\boldsymbol{\pi}^*, \Theta_{x,c}^*, c = 1, \dots, C\}$ randomly;

Repeat:

E-Step:

Calculate $\mathbb{E}_\omega[\omega_{c,i} | \mathcal{S}; \Omega^*]$ as (9);

Calculate $\mathbb{E}_\omega[A_c^{r,r'}(s, t) | \mathcal{S}; \Omega^*]$ and $\mathbb{E}_\omega[B_c^r(t) | \mathcal{S}; \Omega^*]$ as linear combinations of $\mathbb{E}_\omega[\omega_{c,i} | \mathcal{S}; \Omega^*]$'s.

S-Step:

Update $\boldsymbol{\pi}^*, \mu_{x,c}^{r*}(t)$ and $\Gamma_{x,c}^{r,r'*}(s, t)$ according to (12), (13) and (14);

End;

Until: Reach the convergence criteria;

$\hat{\boldsymbol{\pi}} = \boldsymbol{\pi}^*, \hat{\mu}_{x,c}^r = \mu_{x,c}^{r*}(t)$ and $\hat{\Gamma}_{x,c}^{r,r'}(s, t) = \Gamma_{x,c}^{r,r'*}(s, t)$;

Model Selection. Algorithm 1 requires choosing a proper number of clusters C and bandwidth h . In model-based clustering, one popular method for choosing the number of clusters is based on the Bayes information criterion (BIC) [26], which can be readily computed for our model since the probability $f(\mathcal{S} | \boldsymbol{\omega})$ is already calculated in each iteration. The choice of bandwidth h also plays an important role in model estimation. A small h may produce unstable clustering results while a large h would dampen the characteristics of each cluster. With $a_i^{r,r'}(s, t; h)$'s and $b_i^r(s; h)$'s given in (7) pre-calculated for different candidates of h , we can adaptively choose the h that maximizes the likelihood in each iteration in a computationally efficient manner.

4.2 Learning of Multi-level Models

We now consider developing the learning algorithm for the multi-level model (1), assuming we repeatedly observe R types of events from n accounts on m days with $m > 1$. Below, we propose a method to transform the learning task of a multi-level model into a problem that can be solved by a two-step procedure, where the second step is mathematically equivalent to a single-level model and hence can be conveniently solved by a similar algorithm as in Algorithm 1.

For a given account i , consider the aggregated event sequence $\bar{S}_i^r = \cup_{j=1}^m S_{i,j}^r$ for each row of \mathcal{S} and event type r . If we assume a multi-level model for each $S_{i,j}^r$ as in (1), conditional on latent variables \mathcal{L} , \bar{S}_i^r is a superposition of m independent Poisson processes and hence can be viewed as a new Poisson process with intensity functional $\lambda_i^r(t | \mathcal{L}) = \sum_{j=1}^m \exp \Lambda_{i,j}^r(t)$. We approximate the distribution of \bar{S}_i^r by a Poisson process with a marginal intensity function,

$$\bar{\lambda}_i^r(t) = \mathbb{E}_{YZ} \{ \lambda_i^r(t | \mathcal{L}) | X_i(t) \} = m \exp \{ \tilde{X}_i^r(t) \}, \quad (15)$$

where $\tilde{\mathbf{X}}_i = \{ \tilde{X}_i^1, \dots, \tilde{X}_i^R \}$ is a new multivariate mixture Gaussian process with mean function $\tilde{\mu}_{x,c}^r(t) = \mu_{x,c}^r + \Gamma_y^{r,r}(t, t)/2 + \Gamma_z^{r,r}(t, t)/2$ and covariance function $\tilde{\Gamma}_{x,c}^{r,r'}(s, t) = \Gamma_{x,c}^{r,r'}(s, t)$, if account i belongs to cluster c . When m is large, we expect the above approximation to be accurate.

Note that the model in (15) for the aggregated event sequence \bar{S}_i^r is inherently reduced to a single-level model. It allows us to separate the inference of the multi-level model in (1) into two steps: (*Step I*) learn the parameters in Θ_y and Θ_z and denote the estimated parameters as $\hat{\Gamma}_y^{r,r'}(s, t)$ and $\hat{\Gamma}_z^{r,r'}(s, t)$; (*Step II*) learn the clusters of the single-level model in (15) and estimate the parameters π , $\tilde{\mu}_{x,c}^r$ and $\tilde{\Gamma}_{x,c}^{r,r'}$. Afterwards, the parameters involved in $\Theta_{x,c}$ can be obtained by

$$\hat{\mu}_{x,c}^r(t) = \tilde{\mu}_{x,c}^r(t) - \hat{\Gamma}_y^{r,r'}(t, t)/2 - \hat{\Gamma}_z^{r,r'}(t, t)/2, \quad \hat{\Gamma}_{x,c}^{r,r'}(s, t) = \tilde{\Gamma}_{x,c}^{r,r'}(s, t).$$

For the learning task in Step I, [32] developed a semi-parametric algorithm to learn the repeatedly observed event sequences. In analogy to their work, we propose a similar inference framework to estimate Θ_y and Θ_x in our mixture multi-level model (1) and provide the details in Supplementary S.1. For step II, we resort to the single-level model algorithm described in Section 4.1.

4.3 Computational Complexity and Acceleration

Assume that the training event sequences belong to n accounts and C clusters and are repeatedly observed on m time slots. We also assume that the data contains R types of events and each sequence consists of I time stamps on average. Let Q be the sampling size used in the Monte Carlo integration in (10). In numerical implementation, we divide the interval $[0, T]$ into D equally spaced grid points $\mathcal{D} = \{0 = u_1 < \dots < u_D = T\}$. In Step I, it requires $O(nmR^2D^2)$ computation complexity to estimate Θ_y and Θ_z , according to [32]. Computation complexity to pre-calculate $a_i^{r,r'}(s, t; h)$'s and $b_i^r(t; h)$'s in (7) for all $s, t \in \mathcal{D}$ is of the order $O(nmR^2D^2)$ if we decompose $a_i^{r,r'}(s, t; h)$ as:

$$a_i^{r,r'}(s, t; h) = \left[\sum_{u \in S_i^r} \frac{K_h(s-u)}{g(s; h)} \right] \left[\sum_{v \in S_i^{r'}} \frac{K_h(t-v)}{g(t; h)} \right] - \sum_{u \in S_i^r \cap S_i^{r'}} \frac{K_h(s-u)K_h(t-v)}{g(s; h)g(t; h)}.$$

In Step II, for each E-S iteration, we need $O(CQR^3)$ for sampling and $O(nCIQR^2)$ for other calculations. Therefore, the overall computational complexity is $O(R^2(nmD^2 + CQR + nCIQ))$. To further reduce computation, we use array programming and GPU acceleration to calculate the high-dimensional integration in the Monte Carlo EM framework [30] to reduce the runtime of (9). The details are included in Supplementary S.2, and a numerical demonstration is given in Section 5.1.

5 Numerical Examples

We examine the performance of our **MM-MPP** framework for clustering event sequences via synthetic data examples and real-world applications and compare the performances between the proposed method and two other state-of-the-art methods. One competing method is a discrete Fréchet distance-based method (**DF**) by [22]. Unlike other distance-based clustering methods, the DF cluster can characterize interactions among events. Another is a model-based clustering method based on the Dirichlet mixture of Hawkes processes (**DMHP**) by [34]. DMHP is chosen as a competitor due to its capability of accounting for complex point patterns while performing clustering and making efficient variational Bayesian inference algorithms under a nested EM framework.

5.1 Synthetic Data

Setting. We generate the synthetic data from the proposed mixture model of log-Gaussian Cox processes in (1) and (2), in which there are $R = 5$ event types and daily time stamps reside in $[0, 2]$. We set the number of clusters C from 2 to 5 and set the number of accounts in each cluster to 500. We experiment with an increasing number of replicates ($m = 1, 20$ or 100), to check the convergence of our method. When $m = 1$, we generate event sequences from the single-level model in (2) without day-level variations. In this case, we compare the clustering results of DF, DMHP with those of the single-level model (MS-MPP). When $m = 20$ or 100 , we generate data from the multi-level model in (1) and use the MM-MPP method to model the scenario where event sequences are repeatedly observed. However, the two competing methods, DF and DMHP, are not directly applicable for repeated event sequences. Therefore, in this case, we concatenate $\{S_{i,j}^r\}_{j=1}^m$ sequentially into a new event sequence S_i^r on $[0, mT]$ and then apply DF and DMGP to this new sequence. The detailed

settings of $X_i^T(t)$'s, $Y_j^T(t)$'s and $Z_{i,j}^T(t)$'s and other details of synthetic data examples are elaborated in Supplementary S.3.

Results. We evaluate the clustering performance of each method over 100 repeated experiments under each setting, using *clustering purity* [25] as a evaluation metric. Table 1 reports the averaged clustering purity of each method on the synthetic data. When $m = 1$, MS-MPP obtains the best clustering result in terms of purity consistently across different numbers of clusters. Especially when C increases, in which case there are more overlaps among clusters, the advantage of MS-MPP becomes more prominent. When $m = 20, 100$, MM-MPP still significantly outperforms the other two competitors. It is also noticeable that the performance of DF and DMPH, in general, deteriorates as m increases, although more repeated event sequences offer more information for clustering. One explanation is that both DF and DMHP may incur bias due to ignoring different sources of variations for repeatedly observed event times. Another reason may be that many existing Hawkes process models, such as DMHP, assume a constant triggering function over time, which may not be flexible enough to characterize the data generated from models (1) and (2).

Table 1: Clustering Purity on Synthetic Data.

C	$m = 1$			$m = 20$			$m = 100$		
	DF	DMPH	MS-MPP	DF	DMPH	MM-MPP	DF	DMPH	MM-MPP
2	0.597	0.537	0.831	0.536	0.513	0.947	0.532	0.522	0.988
3	0.514	0.466	0.767	0.465	0.423	0.902	0.477	0.394	0.967
4	0.443	0.421	0.714	0.422	0.356	0.874	0.436	0.285	0.944
5	0.379	0.354	0.675	0.351	0.298	0.835	0.333	0.276	0.919

Our code can be accessed via <https://github.com/LihaoYin/MMPP>. To show the computational advantage of the proposed ES algorithm over the EM algorithm, Table 2 gives the computation times of CPU-based EM, CPU-based ES, and GPU-based ES algorithms for 20 iterations in the estimation of model (1) with $n = 500, 100$, $m = 20$, $R = 5$ and $C = 3$. For each iteration, 10,000 MCMC samples are drawn to approximate (10). Table 2 demonstrates that with the GPU acceleration, the computation time of the proposed ES can be reduced by more than 20 folds in this case scenario compared to the EM algorithm, which is not suitable for array programming [8].

Table 2: Running Time (in seconds) on Synthetic Data

Methods and devices	$n = 500$	$n = 1000$
GPU-ES (RTX 8000 48G GPU)	30.09	51.42
CPU-ES (i7-7700HQ CPU)	275.87	505.07
CPU-EM (i7-7700HQ CPU)	568.36	1105.46

5.2 Real-world Data

In this section, we apply our method to the following real-world datasets.

Twitter Dataset. The Twitter dataset consists of the postings of the official accounts of America’s top 500 universities from April 15, 2021, to May 14, 2021. The data set was scraped from Twitter with the API `rtweet` [13]. The dataset involves three categories of postings (tweet, retweet, and reply), indicating $R = 3$ in this study. As a result, the dataset contains $n = 500$ Twitter accounts for $m = 30$ consecutive days with a total of 233,465 time stamps.

Chicago City Taxi Dataset The City of Chicago collected the information of all taxi rides in Chicago since 2013¹. Each trip record in the dataset consists of drivers’ encrypted IDs, pick-up/drop-off time stamps, and locations (in the form of latitude/longitude coordinates). We gathered the trips of 9,000 randomly selected taxi drivers from Jan 1 to Dec 31, 2016, and more than 19 million trip records were picked. We mapped the pick-up coordinates to their corresponding zoning types according to Chicago Zoning Map Dataset², which divides the city into nine basic zoning districts³, including Residence (R), Business (B), Commercial (C), Manufacturing (M), etc. For this data set, we have $n = 9000$, $m = 366$, and $R = 9$.

¹<https://data.cityofchicago.org/Transportation/Taxi-Trips/wrvz-psew>

²<https://data.cityofchicago.org/>

³<https://secondcityzoning.org/zones/>

Credit Card Transaction Dataset. The dataset contains 641,914 transaction records of 5,000 European credit card customers ($n = 5000$) during the period covering January 1 to December 31, 2016 ($m = 366$). We applied the univariate model ($R = 1$) without event marks to the dataset.

We evaluate and compare clustering stability based on a measure called *clustering consistency* via K -trial cross-validations [27, 28], as there are no ground truth clustering labels. The detailed definition of *clustering consistency* and other real data example details are included in Supplementary S.4.

Results. We compare the performance of DF, DMHP, and MM-MPP in terms of clustering consistency for three data sets with $K = 100$ trials. The results in Table 3 suggest that MM-MPP outperforms its competitors notably, demonstrating that our model can better characterize the postings patterns and offer a more stable and consistent clustering than other methods. Figure 2 shows the histograms of the number of learned clusters for each method. For the Twitter dataset, the median numbers of learned clusters are 3, 5, and 8 for MM-MPP, DMHP, and DF respectively. Besides, the distribution of the number of clusters from our method seems to be the least variable, indicating robustness in clustering. The robustness of our method may be partly attributed to the flexibility of the latent conditional intensity functions that account for multi-level deviations within each account. In contrast, other methods that fail to account for different sources of deviations may treat them as sources of heterogeneity and consequently result in more clusters.

Table 3: Clustering Consistency on Real-World Datasets.

Method	DF	DMHP	MM-MPP
Twitter	0.096	0.275	0.394
Credit Card	0.102	0.331	0.378
Chicago Taxi	0.045	0.142	0.153

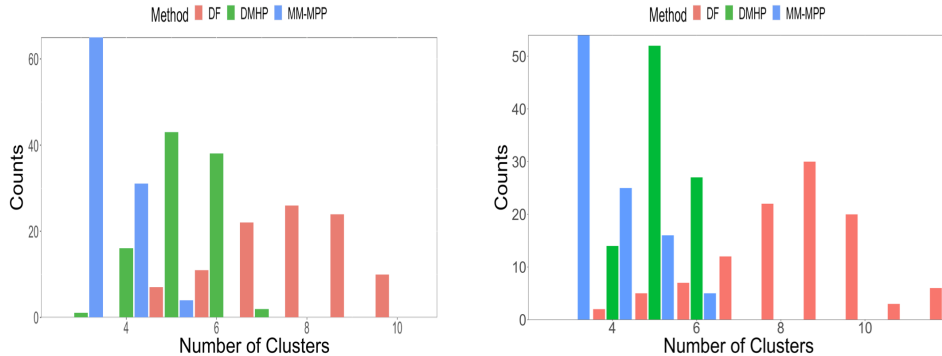


Figure 2: Histogram of the number of clusters. Left: Twitter dataset; Right: Credit Card dataset;

More stories can be told by the estimated posting patterns. Given a predicted membership of account i by $c_i = \arg \max_c \mathbb{E}_\omega[\omega_{c,i} | \mathcal{S}; \hat{\Omega}]$, Figure 3 displays the estimated curves of $\hat{\mu}_{x,c}^r$ for tweet events ($r = 1$), retweet events ($r = 2$) and reply events ($r = 3$) respectively for $C = 3$. Recall $\hat{\mu}_{x,c}^r$ is interpreted as the baseline of intensity functions. This figure shows three different activity modes for the selected Twitter accounts. The universities in cluster 1 marked by red curves in Figure 3 in general have a lower frequency of posting retweets and replies, especially during the daytime. This group includes the most top university in America, such as MIT, Harvard, and Stanford. In contrast, the accounts in cluster 2 are relatively more active in all three types of postings. We further find that many accounts in this cluster belong to the universities with middle ranks.

We further applied the proposed MM-MPP to the Chicago Taxi dataset. As suggested by BIC, the 9000 taxi drivers are clustered into 9 groups, whose averaged daily pick-up log intensity functions are illustrated in Figure 4(a). We can see that the taxi drivers are clustered not only according to their pick-up frequency but also by their working schedules. For example, the black curves on Figure 4(a) corresponds to the most dominating group, which occupies 23.2% of the sample. Figure 3(b) displays the curves of average log intensity (the black line) and log intensity for each driver (gray lines) in the selected cluster. Figure 4(c-e) show the estimated $\hat{\mu}_x(t)$ for pick-up in commercial, residence and

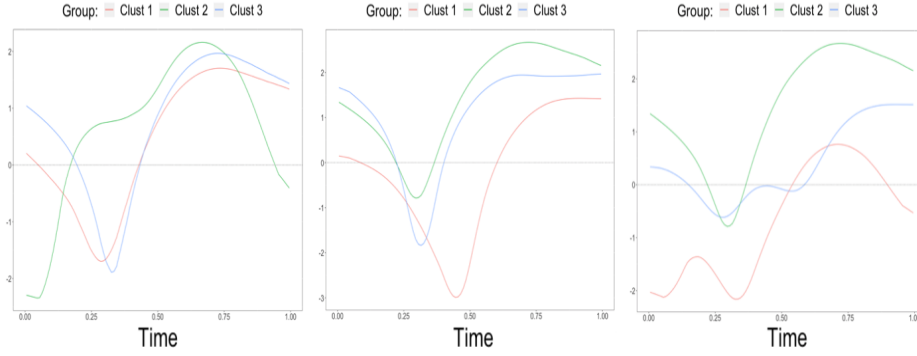


Figure 3: Curves of $\hat{\mu}_{x,c}^r(t)$. Left: tweet events; Mid: retweet events; Right: reply events;

manufacturing districts, respectively. While the pick-up events are more likely to occur in commercial districts for this group during the daytime, they also tend to pick up passengers at the residential district in the morning and to appear at the manufacturing district in the afternoon. These patterns are consistent with the schedules of passengers who commute between homes and workplaces.

More results and discussions on chase credit dataset are included in our Supplementary file.

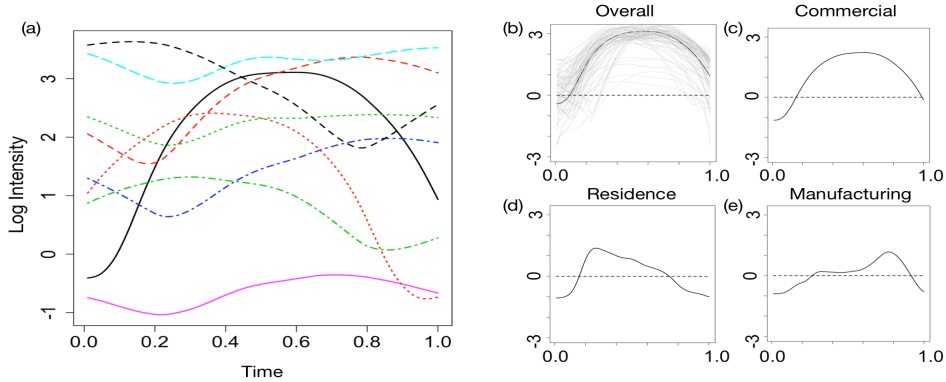


Figure 4: Left: Overall log-intensities for all clusters; Right: Log-intensity for one selected cluster;

6 Concluding Remarks

We propose a mixture of multi-level marked point processes to cluster repeatedly observed marked event sequences. A novel and efficient learning algorithm is developed based on a semi-parametric ES algorithm. The proposed method is demonstrated to significantly outperform other competing methods in simulation experiments and real data analyses.

The current model only focuses on events over temporal domains. However, clustering of spatial patterns on 2- or 3-dimensional domains has also attracted much research interest [11, 35, 10]. It will be an interesting research topic to extend the current model to such settings.

This work has no foreseeable negative societal impacts, but users should be cautious when giving interpretation on clustering results to avoid any misleading conclusions.

Acknowledgement

We thank the anonymous reviewers for their constructive comments that help improve the manuscript significantly. Xu’s research is supported by NSF grant SES-1902195, Guan’s research is supported by NSF grant SES-1758575, and Sang’s research is supported by NSF grant DMS-1854155.

7 Supplementary Files

Abbreviations

- **ES**: Expectation-Solution;
- **LGCP**: log-Gaussian Cox process;
- **FPCA**: Functional principal component analysis;
- **MM-MPP**: Mixture Multi-level Marked Point Processes;
- **MS-MPP**: Mixture Single-level Marked Point Processes;
- **MC**: Monte Carlo
- **DMHP**: Dirichlet mixture of Hawkes processes;
- **DF**: discrete Fréchet;

7.1 Step I of the Two-step Learning of the Multi-Level Model

We consider a multi-level model with the following latent intensity function:

$$\lambda_{i,j}^r(t) = \exp\{X_i^r(t) + Y_j^r(t) + Z_{i,j}^r(t)\}, \quad t \in [0, T] \quad (16)$$

for $i = 1, \dots, n, j = 1, \dots, m$ and $r = 1, \dots, R$.

As discussed in Section 4.2, the learning algorithm is decomposed into two steps as in Algorithm 2. In Step I, we seek to estimate the parameters in Θ_y and Θ_z . Other cluster-specific model parameters such as cluster assignment probabilities π are estimated in Step II following the procedure described in Section 4.2. [32] developed a semi-parametric algorithm to estimate the covariance functions of a multi-level log-Gaussian Cox process. We extend their estimation method to also take into account unknown clustering when estimating Θ_y and Θ_z in Step I. Interestingly, we will show that the resulting estimators of Θ_y and Θ_z do not depend on any other cluster-specific parameters and hence avoid iterations between the two steps.

Specifically, following the formula of the moment generating function of a Gaussian random variable, the marginal intensity functions can be calculated as

$$\rho^r(t) = \mathbb{E}[\lambda_{i,j}^r(t)] = \sum_{c=1}^C \pi_c \exp\{\mu_{x,c}^r(t) + \Gamma_{x,c}^{r,r}(t, t)/2 + \Gamma_y^{r,r}(t, t)/2 + \Gamma_z^{r,r}(t, t)/2\},$$

and derived in a similar way, the marginal second-order intensity functions are:

$$\begin{aligned} \rho_{i,j,i',j'}^{r,r'}(s, t) &= \mathbb{E}[\lambda_{i,j}^r(s) \lambda_{i',j'}^{r'}(t)] \\ &= \sum_c \sum_{c'} \mathbb{E}[\exp\{Y_j^r(s) + Y_{j'}^{r'}(t) + Z_{i,j}^r(s) + Z_{i',j'}^{r'}(t)\}] \\ &\quad \cdot \mathbb{E}[\omega_{c,i} \omega_{c',i'}] \cdot \mathbb{E}[\exp\{X_i^r(s) + X_{i'}^{r'}(t)\} | \omega_{c,i} = 1, \omega_{c',i'} = 1] \end{aligned}$$

for $i, i' = 1, \dots, n, j, j' = 1, \dots, m$ and $r, r' = 1, \dots, R$.

We analyze the form of $\rho_{i,j,i',j'}^{r,r'}$ under four different situations and use $A^{r,r'}$, $B^{r,r'}$, $C^{r,r'}$ or $D^{r,r'}$ to represent its form under each situation respectively,

$$\rho_{i,j,i',j'}^{r,r'}(s, t) = \begin{cases} A^{r,r'}(s, t) \equiv \exp\{\Gamma_y^{r,r'}(s, t) + \Gamma_z^{r,r'}(s, t)\} \sum_c \pi_c \rho_c^r(s) \rho_c^{r'}(t) \exp\{\Gamma_{x,c}^{r,r'}(s, t)\}, & \text{if } i = i', j = j' \\ B^{r,r'}(s, t) \equiv \sum_c \pi_c \rho_c^r(s) \rho_c^{r'}(t) \exp\{\Gamma_{x,c}^{r,r'}(s, t)\}, & \text{if } i = i', j \neq j' \\ C^{r,r'}(s, t) \equiv \exp\{\Gamma_y^{r,r'}(s, t)\} \sum_{c,c'} \pi_c \pi_{c'} \rho_c^r(s) \rho_{c'}^{r'}(t), & \text{if } i \neq i', j = j' \\ D^{r,r'}(s, t) \equiv \sum_{c,c'} \pi_c \pi_{c'} \rho_c^r(s) \rho_{c'}^{r'}(t), & \text{if } i \neq i', j \neq j' \end{cases} \quad (17)$$

It can be seen that $A^{r,r'}(s, t)$, $B^{r,r'}(s, t)$, $C^{r,r'}(s, t)$ and $D^{r,r'}(s, t)$ captures different correlation information, namely, the correlation within same-account same-day, within same-account across different-day, within same-day across different-account, and across different-account different-day, while integrating out the unknown cluster memberships of i and i' .

Following a similar derivation as [32], the corresponding empirical kernel estimate of $\rho_{i,j,i',j'}^{r,r'}$ under each situation is given by

$$\left\{ \begin{array}{l} \hat{A}^{r,r'}(s, t; h) = \sum_{i=1}^n \sum_{j=1}^m \sum_{\substack{u \neq v \\ u \in S_{i,j}^r, v \in S_{i,j}^{r'}}} \frac{K_h(s-u)K_h(t-v)}{nmg(s;h)g(t;h)} \\ \hat{B}^{r,r'}(s, t; h) = \sum_{i=1}^n \sum_{j=1}^m \sum_{j' \neq j} \sum_{u \in S_{i,j}^r} \sum_{v \in S_{i,j'}^{r'}} \frac{K_h(s-u)K_h(t-v)}{nm(m-1)g(s;h)g(t;h)} \\ \hat{C}^{r,r'}(s, t; h) = \sum_{i=1}^n \sum_{i' \neq i} \sum_{j=1}^m \sum_{u \in S_{i,j}^r} \sum_{v \in S_{i',j}^{r'}} \frac{K_h(s-u)K_h(t-v)}{n(n-1)mg(s;h)g(t;h)} \\ \hat{D}^{r,r'}(s, t; h) = \sum_{i=1}^n \sum_{i' \neq i} \sum_{j=1}^m \sum_{j' \neq j} \sum_{u \in S_{i,j}^r} \sum_{v \in S_{i',j'}^{r'}} \frac{K_h(s-u)K_h(t-v)}{n(n-1)m(m-1)g(s;h)g(t;h)} \end{array} \right. \quad (18)$$

for $r, r' = 1, \dots, R$, where $K_h(t) = h^{-1}K(t/h)$ is a kernel function with bandwidth h and $g(x; h) = \int K_h(x-t)dt$ is an edge correction term.

Matching (17) with (18), we propose to estimate the covariance functions using,

$$\hat{\Gamma}_y^{r,r'}(s, t; h) = \log \frac{\hat{C}^{r,r'}(s, t; h)}{\hat{D}^{r,r'}(s, t; h)}, \quad \hat{\Gamma}_z^{r,r'}(s, t; h) = \log \frac{\hat{A}^{r,r'}(s, t; h)\hat{D}^{r,r'}(s, t; h)}{\hat{B}^{r,r'}(s, t; h)\hat{C}^{r,r'}(s, t; h)} \quad (19)$$

Algorithm 2 Learning of the Multi-level model (1)

Input: $\mathcal{S} = \{S_{i,j}^r\}$, the number of clusters C , the bandwidth h ;

Output: Estimates of model parameters, $\hat{\pi}$, $\hat{\Theta}_y$, $\hat{\Theta}_z$, $\hat{\Theta}_{x,c}$, for $c = 1, \dots, C$;

Step I: Given \mathcal{S} , obtain $\hat{\Theta}_y$ and $\hat{\Theta}_z$ using the estimation framework in Section 7.1;

Step II:

- a) Aggregate the event sequences by $\bar{S}_i^r = \cup_{j=1}^m S_{i,j}^r$;
- b) Based on $\{\bar{S}_i^r\}_{i=1}^n$ from a), fit the single-level model with parameters $\{\pi, \tilde{\Theta}_{x,c}\}$ using Algorithm 1;
- c) Calculate,

$$\hat{\mu}_{x,c}^r(t) = \tilde{\mu}_{x,c}^r(t) - \hat{\Gamma}_y^{r,r}(t, t)/2 - \hat{\Gamma}_z^{r,r}(t, t)/2 - \log m, \quad \hat{\Gamma}_{x,c}^{r,r'}(s, t) = \tilde{\Gamma}_{x,c}^{r,r'}(s, t)$$

7.2 Computational Details

7.2.1 ES Algorithm

The Expectation-Solution (ES) algorithm [7, 18] is a general extension of the Expectation-Maximization (EM) algorithm. It is an iterative approach built upon estimating equations that involve missing data or unobserved variables. In the E-step of each iteration, ES calculates the conditional expectations of estimating equations given observed data and current parameter estimates. In S-step, it updates parameter values by finding the solutions to the expected estimating equations. Since the estimating equations can be constructed from a likelihood, a quasi-likelihood, or other forms, the ES algorithm is more flexible and general than the EM algorithm. In particular, when estimating equations are well designed such that analytical solutions are available in S-step, ES algorithm may achieve an improved computational efficiency over EM algorithms, which often involve expensive numerical optimizations of the expected log-likelihood in each M-step.

We follow the notations and expressions in [7]. Let \mathbf{y} denote the observed data vector, \mathbf{z} denote the unobserved data, and $\mathbf{x} = \{\mathbf{y}, \mathbf{z}\}$ be the complete-data. Let $\boldsymbol{\Omega}$ denote a d -dimensional vector of parameters. Given d -dimensional estimating equations with the complete data as:

$$U_c(\mathbf{x}; \boldsymbol{\Omega}) = \mathbf{0}$$

the ES algorithm entails a linear decomposition like:

$$\begin{aligned} U_c(\mathbf{x}; \boldsymbol{\Omega}) &= U_1(\mathbf{y}, \mathbf{S}(\mathbf{x}); \boldsymbol{\Omega}) \\ &= \sum_{j=1}^q \mathbf{a}_j(\boldsymbol{\Omega}) S_j(\mathbf{x}) + \mathbf{b}_\Omega(\mathbf{y}), \end{aligned} \quad (20)$$

where \mathbf{a}_j 's are vectors of size d only depending on parameters $\boldsymbol{\Omega}$, and \mathbf{S} is a q -dimensional function with components S_j only depending on the complete data. $\mathbf{S}(\mathbf{x})$ is referred to as a "complete-data summary statistic". Given the parameters $\boldsymbol{\Omega}^*$, we calculate the expectation over \mathbf{z} condition on \mathbf{y} and parameters $\boldsymbol{\Omega}$ in E-step as following

$$h(\mathbf{y}; \boldsymbol{\Omega}^*) = \mathbb{E}_z[\mathbf{S}(\mathbf{x})|\mathbf{y}; \boldsymbol{\Omega}^*]$$

In view of the linearity in (20), we consider the conditionally expected estimation equations,

$$\mathbb{E}_z[U_c(\mathbf{x}; \boldsymbol{\Omega})|\mathbf{y}; \boldsymbol{\Omega}^*] = U_1(\mathbf{y}, h(\mathbf{y}; \boldsymbol{\Omega}^*); \boldsymbol{\Omega}) = \mathbf{0} \quad (21)$$

In the S-step, we update the parameters $\boldsymbol{\Omega}$ by finding the solution to (21). We outline the ES procedure in Algorithm 3.

Algorithm 3 ES Algorithm

Presupposition: Given estimating equations $U_c(\mathbf{x}; \boldsymbol{\Omega})$ with a linear decomposition (20);

Input: Observed data \mathbf{y} ;

Output: Estimates of model parameters $\boldsymbol{\Omega}$;

Initialize $\boldsymbol{\Omega}^*$ randomly;

Repeat:

E-Step: Calculate $h(\mathbf{y}; \boldsymbol{\Omega}^*) = \mathbb{E}_z[\mathbf{S}(\mathbf{x})|\mathbf{y}; \boldsymbol{\Omega}^*]$;

S-Step: Find $\boldsymbol{\Omega}$ that solve $U_1(\mathbf{y}, h(\mathbf{y}; \boldsymbol{\Omega}^*); \boldsymbol{\Omega}) = \mathbf{0}$ in (21);

End;

Until: Reach the convergence criteria.

7.2.2 Sampling Strategy

The E-step in Section 4.1 involves the sampling of random functions $\mathbf{X}_c^{(q)}$ for calculating the Monte Carlo integration in (10). Given cluster-specific parameters $\Omega_{x,c}$, our goal is to draw multiple independent realizations of $\mathbf{X}_i(t)|\omega_{c,i} = 1$, denoted as $\mathbf{X}_c^{(q)}(t) = \{X_c^{1(q)}(t), \dots, X_c^{R(q)}(t)\}'$. Recall that the cross covariance functions of $\mathbf{X}_i(t)$ is $\Gamma_{x,c}^{r,r'}(s, t) = \text{Cov}[X_i^r(s), X_i^{r'}(t)|\omega_{c,i} = 1]$, $s, t \in [0, T]$, for $i = 1, \dots, n$. When $r = r'$, the covariance function $\Gamma_{x,c}^{r,r}(s, t)$ is a symmetric, continuous and nonnegative definite kernel function on $[0, T] \times [0, T]$. Then Mercer's theorem asserts that there exists the following spectral decomposition:

$$\Gamma_{x,c}^{r,r}(s, t) = \sum_{k=1}^{\infty} \eta_{x,c,k}^r \phi_{x,c,k}^r(s) \phi_{x,c,k}^r(t),$$

where $\eta_{x,c,1}^r \geq \eta_{x,c,2}^r \geq \dots > 0$ are eigenvalues of $\Gamma_{x,c}^{r,r}(s, t)$ and $\phi_{x,c,k}^r(t)$'s are the corresponding eigenfunctions which are pairwise orthogonal in $L^2([0, T])$. The eigenvalues and eigenfunctions satisfy the integral eigenvalue equation,

$$\eta_{x,c,k}^r \phi_{x,c,k}^r(s) = \int_0^T \Gamma_{x,c}^{r,r}(s, t) \phi_{x,c,k}^r(t) dt$$

Accordingly, using the Karhunen-Loève expansion [29], $X_c^{r(q)}(t)$ admits a decomposition,

$$X_c^r(t) = \mu_{x,c}^r(t) + \sum_{k=1}^{\infty} \xi_{x,c,k}^r \phi_{x,c,k}^r(t), \quad (22)$$

where $\{\xi_{x,c,k}^r\}_{k=1}^{\infty}$ are independent normal random variables with mean 0 and variance $\{\eta_{x,c,k}^r\}_{k=1}^{\infty}$. The expression in (22) has an infinite dimensional parameter space, which is infeasible for estimation. One solution is to approximate (22) by only keeping leading principal components,

$$X_c^r(t) \approx \mu_{x,c}^r(t) + \sum_{k=1}^{p_c^r} \xi_{x,c,k}^r \phi_{x,c,k}^r(t) \quad (23)$$

where p_c^r is a rank chosen to characterize the dominant characteristics of X_c^r while reducing computational complexity. It leads to a reduced-rank representation of $\Gamma_{x,c}^{r,r}(s, t)$ as:

$$\Gamma_{x,c}^{r,r}(s, t) \approx \sum_{k=1}^{p_c^r} \eta_{x,c,k}^r \phi_{x,c,k}^r(s) \phi_{x,c,k}^r(t).$$

Similarly, when $r \neq r'$, we can also approximate $\Gamma_{x,c}^{r,r'}(s, t)$ using the truncated decomposition,

$$\Gamma_{x,c}^{r,r'}(s, t) \approx \sum_{k=1}^{p_c^r} \sum_{k'=1}^{p_c^{r'}} \eta_{x,c,k,k'}^{r,r'} \phi_{x,c,k}^r(s) \phi_{x,c,k'}^{r'}(t). \quad (24)$$

We denote $\xi_{x,c}^r = \{\xi_{x,c,1}^r, \dots, \xi_{x,c,p_c^r}^r\}'$ and investigate the cross-covariance matrix of $\xi_{x,c} = \{\xi_{x,c}^1, \dots, \xi_{x,c}^R\}$, denoted as

$$\Sigma_{x,c} = \begin{pmatrix} \Sigma_{x,c}^{1,1} & \dots & \Sigma_{x,c}^{1,R} \\ \vdots & \ddots & \vdots \\ \Sigma_{x,c}^{R,1} & \dots & \Sigma_{x,c}^{R,R} \end{pmatrix},$$

where $\Sigma_{x,c}^{r,r'} = \text{Cov}[\xi_{x,c}^r, \xi_{x,c}^{r'}]$.

From Karhunen-Loève expansion in (22), we know $\Sigma_{x,c}^{r,r} = \text{diag}(\eta_{x,c,1}^r, \dots, \eta_{x,c,p_c^r}^r)$ for each event type r . When $c \neq c'$, we assume that $\xi_{x,c}^r$ and $\xi_{x,c'}^{r'}$ are independent. However, when considering two different event types (i.e., $r \neq r'$) within the same cluster, it is reasonable to account for the correlation between $\xi_{x,c}^r$ and $\xi_{x,c}^{r'}$ to characterize interactions among events of different types. Therefore, from (22) and (24), the (k, k') -th entry of the covariance matrix $\Sigma_{x,c}^{r,r'}$ is $\eta_{x,c,k,k'}^{r,r'}$ when $r \neq r'$.

Now we can draw the samples $\xi_{x,c}^{(q)} = \{\xi_{x,c}^{1(q)}, \dots, \xi_{x,c}^{R(q)}\}$ from the multivariate normal distribution with a mean zero and a covariance matrix is $\Sigma_{x,c}$, based on which we obtain the samples $X_c^{(q)}$ using expansion (23).

7.2.3 GPU Acceleration

One computational bottleneck in our approach is the Monte Carlo (MC) approximation of the high-dimensional integration in (10). Although we have employed the low-rank representations by FPCA in Section 7.2.2 to facilitate MC sampling, this step remains as the most computationally expensive part if using a naive direct calculation, due to the massive number of sampling points for a precise MC integration.

Many researchers have embarked their efforts on improving the performance of MC integration. One of the most popular frameworks is VEGAS [15, 21] due to its user-friendly interface. However, VEGAS, which is CPU-based, may be over-stretched with dimensionality going up since the required MC samples consequently increase dramatically. As notable progress, GPU-based programs, like VegasFlow[5], extremely boosts the computation speed compared to the CPU-version program. It accelerates the computation with the Numpy-like API syntax, such as Tensorflow, which is easy to communicate to GPU. Similar treatments are implemented in our work, and the key is to transfer the

summation loop in (11) into the form of array programming [8]. For example, when we calculate $\mathbf{X}_c^q(t)$ in (23), the computation involves total $p_c^r \times Q$ sampled $\xi_{x,c,k}^r$ and $p_c^r \times I \times n$ of $\phi_{x,c,k}^r(u)$, if given c and r . It will greatly reduce the running time if we utilize array programming. For example, in the case when we have $n = 500$ sequences and 10,000 MC points, our MS-MPP algorithm costs on average 30.09 seconds to run 20 ES iterations on RTX-8000 48G GPU. In contrast, it costs 275.87 seconds on i7-7700HQ CPU if not using array programming.

7.3 Simulation Studies

Setting of $X_i^r(\cdot)$'s. In our synthetic data, we sample event sequences from C heterogeneous clusters ($C = 2, 3, 4$ or 5). Each cluster contains 500 event sequences, and each event sequence contains $R = 5$ event types. We experiment with each setting for $J = 100$ times and investigate the average performance. In each trial, we set,

$$\mu_{x,c}^r(t) = 1 + \sum_{k=0}^{50} \zeta_k Z_{c,k}^r \cos(k\pi t) + \sum_{k=0}^{50} \zeta_k Z_{c,k}^r \sin(k\pi t), \quad t \in [0, 2]$$

for $r = 1, \dots, R$ and $c = 1, \dots, C$, where $Z_{c,k}^r$'s and $Z_{c,k}^r$'s are all independently sampled from the uniform distribution $U(-1, 1)$ and $\zeta_k = (-1)^{k+1} (k+1)^{-2}$. We set the covariance function of $X_i^r(t)$ as,

$$\Gamma_{x,c}^{r,r}(s, t) = \sum_{k=1}^{50} \tilde{Z}_{c,k}^r |\zeta_k| \sin(k\pi s + \pi \tilde{Z}_{c,k}^r) \sin(k\pi t + \pi \tilde{Z}_{c,k}^r)$$

for $r = 1, \dots, R$ and $c = 1, \dots, C$, where $\tilde{Z}_{c,k}^r$'s are independently sampled from uniform distribution $U(0, 0.3)$. Meanwhile, we set the interventions among different event types as,

$$\Gamma_{x,c}^{r,r'}(s, t) = \sum_{k=1}^{50} \sum_{k'=1}^{50} \tilde{Z}_{c,k}^{r,r'} \sqrt{\tilde{Z}_{c,k}^{[j]} \tilde{Z}_{c,k'}^{[j']}} |\zeta_k \zeta_{k'}| \sin(k\pi s + \pi \tilde{Z}_{c,k}^r) \sin(k\pi t + \pi \tilde{Z}_{c,k}^r),$$

for $r \neq r'$, where $\tilde{Z}_{c,k}^{r,r'}$'s are independently sampled from uniform distribution $U(-1, 1)$. The latent variable $X_i^r(t)$'s are generated from Gaussian processes on $[0, 2]$ with the parameters above.

Setting of $Y_j^r(\cdot)$'s and $Z_{i,j}^r(\cdot)$'s. Furthermore, we generate event sequences for m ($m = 1, 20$ or 100) days. When $m = 1$, the event sequences are generated from the single-level model in (2), which didn't involve the variation $Y_j(t)$ and $Z_{i,j}(t)$. When $m = 20$ or 100, we incorporate $Y_j(t)$ and $Z_{i,j}(t)$ in the intensity function and generate data with the multi-level model in (1).

We further describe the setup of the distributions of $Y_j^r(t)$'s and $Z_{i,j}^r(t)$'s. We let,

$$\tilde{Y}_j^r(t) = \sum_{k=1}^2 \xi_{r,j,k}^Y \phi_k^Y(t), \quad Z_{i,j}^r(t) = \sum_{k=1}^4 \xi_{r,i,j,k}^Z \phi_k^Z(t)$$

where $\xi_{r,j,k}^Y$'s and $\xi_{r,i,j,k}^Z$'s are all independent mean-zero normal variables. We set $Var[\xi_{r,j,k}^Y] = 0.2$ and $Var[\xi_{r,i,j,k}^Z] = 0.05$. We set $\{\phi_1^Y(t), \phi_2^Y(t)\} = \{1, \sin(2\pi t)\}$ and $\{\phi_1^Z(t), \phi_2^Z(t), \phi_3^Z(t), \phi_4^Z(t)\} = \{1_{[0,0.5]}, 1_{(0.5,1]}, 1_{(1,1.5]}, 1_{(1.5,2]}\} \times 2 \sin(4\pi t)$. Moreover, in order to model the dependence among different days, we let $Y_j^r(t) = 0.8\tilde{Y}_j^r(t) + 0.6\tilde{Y}_{j-1}^r(t)$ for $j > 1$.

Evaluation Metric. For synthetic data, we introduce the criterion *clustering purity* [25] to evaluate the clustering accuracy.

$$\text{Purity} = \frac{1}{n} \sum_{c=1}^C \max_{j \in \{1, \dots, C\}} |\mathcal{W}_c \cap \mathcal{C}_j|,$$

where \mathcal{W}_c is the estimated index set of sequences belonging to the c th group, \mathcal{C}_j is the true index set of sequence belonging to the j th cluster, and $|\cdot|$ is the cardinality counting the number of elements in a set. The value of *clustering purity* resides in $[0, 1]$ with a higher value indicating a more accurate clustering (=1 if the estimated clusters completely overlap with the truth).

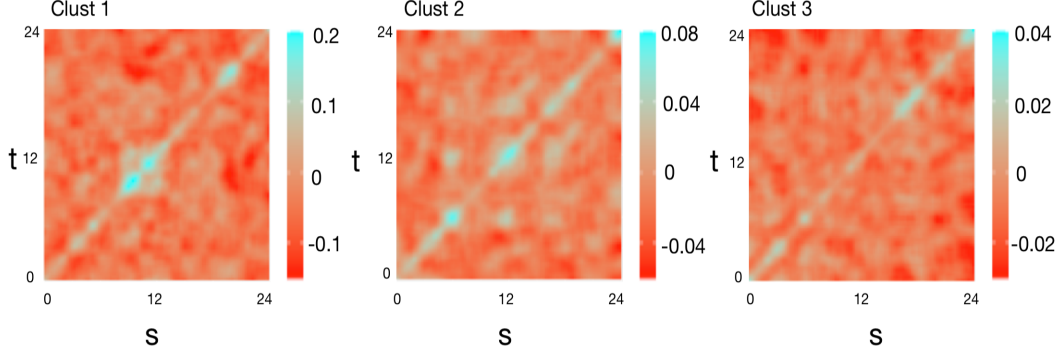


Figure 5: Credit Card Dataset: Estimated $\Gamma_{x,c}(s, t)$ for each cluster;

7.4 Additional Real Data Examples and Details

Evaluation Metric In the real data example, we evaluate and compare clustering stability based on a measure called *clustering consistency* via K -trial cross validations [27, 28], as there is no ground truth clustering labels.

It works with the following rationale: because random sampling does not change the clustering structure of data, a clustering method with high consistency should preserve the pairwise relationships of samples in different trials. Specifically, we perform the clustering with K trials. In the k -th trial, we randomly separate the accounts into two folds. One fold contains 80% of accounts and serves as the training set, and we predict the cluster memberships of remaining accounts with the trained model. Let $\mathcal{M}_k = \{(i, i') | i, i' \text{ belong to the same cluster}\}$ enumerate all pairs of accounts with the same cluster index in the k -th trial. Then we define the *clustering consistency* as:

$$\text{Clustering Consistency} = \min_{k \in \{1, \dots, K\}} \sum_{k' \neq k} \sum_{(i, i') \in \mathcal{M}_k} \frac{1\{c_i^k = c_{i'}^{k'}\}}{|K-1| |\mathcal{M}_k|}$$

where $1\{\cdot\}$ is an indicator function and c_i^j denote the learned cluster index of the account i in the k -th trial.

Additional Results on Chase Credit Card Dataset. In the credit card transaction dataset, there is a large variation in the frequencies in credit card use across users. We removed the users with fewer than 100 total transactions. The BIC suggests clustering the users into 3 groups. In each cluster, we obtained the estimated surface of covariance function $\Gamma_{x,c}(s, t)$, which is displayed in Figure 5. Compared with clust 2 and 3, the latent process $\mathbf{X}_i(t)$ in clust 1 has relatively larger variation. To offer a more straightforward view of the correlation among events, we computed the average correlations as,

$$\overline{\text{Corr}}(r) = \frac{\sum_{|t-s|=r} \widehat{\text{Corr}}(t, s)}{\sum_{|t-s|=r} 1}$$

Where $\widehat{\text{Corr}}(t, s) = \widehat{\Gamma}_{x,c}(t, s) / \sqrt{\widehat{\Gamma}_{x,c}(t, t) \widehat{\Gamma}_{x,c}(s, s)}$. Figure 6 displays the averaged correlations versus time lags. There appears to be a periodic pattern in credit card use for clust 1 and 3. The users in clust 1 seemed to use their credit cards most frequently since the plot of clust 1 has the most number of crests. It is consistent with our facts that users in clust 1 averagely used credit cards 3.7 times a day, versus 1.3 times and 2.2 times a day for clust 2 and 3 respectively.

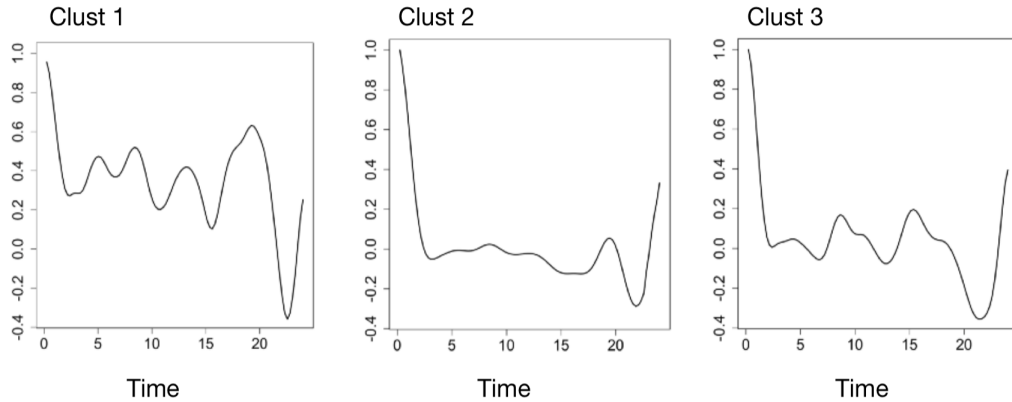


Figure 6: Credit Card Dataset: Averaged correlations versus time lags;

References

- [1] Murray Aitkin and Donald B Rubin. Estimation and hypothesis testing in finite mixture models. *Journal of the Royal Statistical Society: Series B (Methodological)*, 47(1):67–75, 1985.
- [2] Mark Berman and T Rolf Turner. Approximating point process likelihoods with glim. *Journal of the Royal Statistical Society: Series C (Applied Statistics)*, 41(1):31–38, 1992.
- [3] Donald J Berndt and James Clifford. Using dynamic time warping to find patterns in time series. In *Proceedings of the 3rd International Conference on Knowledge Discovery and Data Mining*, pages 359–370, 1994.
- [4] Paul S Bradley and Usama M Fayyad. Refining initial points for k-means clustering. In *ICML*, volume 98, pages 91–99. Citeseer, 1998.
- [5] Stefano Carraza and Juan M Cruz-Martinez. Vegasflow: accelerating monte carlo simulation across multiple hardware platforms. *Computer Physics Communications*, 254:107376, 2020.
- [6] Daryl J Daley and David Vere-Jones. *An introduction to the theory of point processes: volume I: elementary theory and methods*. Springer, 2003.
- [7] Michael Elashoff and Louise Ryan. An EM algorithm for estimating equations. *Journal of Computational and Graphical Statistics*, 13(1):48–65, 2004.
- [8] Charles R Harris, K Jarrod Millman, Stéfan J van der Walt, Ralf Gommers, Pauli Virtanen, David Cournapeau, Eric Wieser, Julian Taylor, Sebastian Berg, Nathaniel J Smith, et al. Array programming with numpy. *Nature*, 585(7825):357–362, 2020.
- [9] Alan G Hawkes and David Oakes. A cluster process representation of a self-exciting process. *Journal of Applied Probability*, pages 493–503, 1974.
- [10] Kristian Bjørn Hessellund, Ganggang Xu, Yongtao Guan, and Rasmus Waagepetersen. Semi-parametric multinomial logistic regression for multivariate point pattern data. *Journal of the American Statistical Association*, pages 1–16, 2021.
- [11] Anders Hildeman, David Bolin, Jonas Wallin, and Janine B Illian. Level set Cox processes. *Spatial statistics*, 28:169–193, 2018.
- [12] Husna Sarirah Husin, Lishan Cui, HERNY Ramadhani Husny Hamid, and Norhaiza Ya Abdullah. Time series analysis of web server logs for an online newspaper. In *Proceedings of the 7th International Conference on Ubiquitous Information Management and Communication*, pages 1–4, 2013.
- [13] Michael W Kearney. rtweet: Collecting and analyzing twitter data. *Journal of Open Source Software*, 4(42):1829, 2019.
- [14] Thomas A Lasko. Efficient inference of gaussian-process-modulated renewal processes with application to medical event data. In *Uncertainty in artificial intelligence: proceedings of the... conference. Conference on Uncertainty in Artificial Intelligence*, volume 2014, page 469. NIH Public Access, 2014.

- [15] G Peter Lepage. A new algorithm for adaptive multidimensional integration. *Journal of Computational Physics*, 27(2):192–203, 1978.
- [16] Liangda Li and Hongyuan Zha. Dyadic event attribution in social networks with mixtures of hawkes processes. In *Proceedings of the 22nd ACM international conference on Information & Knowledge Management*, pages 1667–1672, 2013.
- [17] Dixin Luo, Hongteng Xu, Yi Zhen, Xia Ning, Hongyuan Zha, Xiaokang Yang, and Wenjun Zhang. Multi-task multi-dimensional hawkes processes for modeling event sequences. In *Twenty-Fourth International Joint Conference on Artificial Intelligence*, 2015.
- [18] Geoffrey J McLachlan and Thriyambakam Krishnan. *The EM algorithm and extensions*, volume 382. John Wiley & Sons, 2007.
- [19] Jesper Møller, Anne Randi Syversveen, and Rasmus Plenge Waagepetersen. Log gaussian cox processes. *Scandinavian journal of statistics*, 25(3):451–482, 1998.
- [20] Jesper Moller and Rasmus Plenge Waagepetersen. *Statistical inference and simulation for spatial point processes*. CRC Press, 2003.
- [21] Thorsten Ohl. Vegas revisited: Adaptive monte carlo integration beyond factorization. *Computer physics communications*, 120(1):13–19, 1999.
- [22] Tao Pei, Xi Gong, Shih-Lung Shaw, Ting Ma, and Chenghu Zhou. Clustering of temporal event processes. *International Journal of Geographical Information Science*, 27(3):484–510, 2013.
- [23] Jie Peng, Hans-Georg Müller, et al. Distance-based clustering of sparsely observed stochastic processes, with applications to online auctions. *Annals of Applied Statistics*, 2(3):1056–1077, 2008.
- [24] JO Ramsay and BW Silverman. Principal components analysis for functional data. *Functional data analysis*, pages 147–172, 2005.
- [25] Hinrich Schütze, Christopher D Manning, and Prabhakar Raghavan. *Introduction to information retrieval*, volume 39. Cambridge University Press Cambridge, 2008.
- [26] Gideon Schwarz et al. Estimating the dimension of a model. *Annals of statistics*, 6(2):461–464, 1978.
- [27] Robert Tibshirani and Guenther Walther. Cluster validation by prediction strength. *Journal of Computational and Graphical Statistics*, 14(3):511–528, 2005.
- [28] Ulrike von Luxburg. Clustering stability: An overview. *Machine Learning*, 2(3):235–274, 2009.
- [29] Satoshi Watanabe. Karhunen-loeve expansion and factor analysis: theoretical remarks and application. In *Trans. on 4th Prague Conf. Information Theory, Statistic Decision Functions, and Random Processes Prague*, pages 635–660, 1965.
- [30] Hong-Zhong Wu, Jun-Jie Zhang, Long-Gang Pang, and Qun Wang. Zmcintegral: A package for multi-dimensional monte carlo integration on multi-gpus. *Computer Physics Communications*, 248:106962, 2020.
- [31] Weichang Wu, Junchi Yan, Xiaokang Yang, and Hongyuan Zha. Discovering temporal patterns for event sequence clustering via policy mixture model. *IEEE Transactions on Knowledge and Data Engineering*, 2020.
- [32] Ganggang Xu, Ming Wang, Jiangze Bian, Hui Huang, Timothy Burch, Sandro Andrade, Jingfei Zhang, and Yongtao Guan. Semi-parametric learning of structured temporal point processes. *Journal of machine learning research*, 2020.
- [33] Ganggang Xu, Chong Zhao, Abdollah Jalilian, Rasmus Waagepetersen, Jingfei Zhang, and Yongtao Guan. Nonparametric estimation of the pair correlation function of replicated inhomogeneous point processes. *Electronic Journal of Statistics*, 14(2):3730–3765, 2020.
- [34] Hongteng Xu and Hongyuan Zha. A dirichlet mixture model of hawkes processes for event sequence clustering. *arXiv preprint arXiv:1701.09177*, 2017.
- [35] Fan Yin, Guanyu Hu, and Weining Shen. Analysis of professional basketball field goal attempts via a bayesian matrix clustering approach. *arXiv preprint arXiv:2010.08495*, 2020.
- [36] R Zhang, C Walder, MA Rizoio, and L Xie. Efficient non-parametric bayesian hawkes processes. In *IJCAI International Joint Conference on Artificial Intelligence*, 2019.

- [37] Feng Zhou, Zhidong Li, Xuhui Fan, Yang Wang, Arcot Sowmya, and Fang Chen. Efficient inference for nonparametric hawkes processes using auxiliary latent variables. *Journal of Machine Learning Research*, 21(241):1–31, 2020.